Impact of thermal atomic displacements on the Curie temperature of 3*d* transition metals

A. V. Ruban
Department of Materials Science and Engineering, KTH Royal Institute of Technology, SE-100 44 Stockholm, Sweden and Materials Center Leoben Forschung GmbH, A-8700 Leoben, Austria

O. E. Peil
Materials Center Leoben Forschung GmbH, A-8700 Leoben, Austria

(Received 2 February 2018; revised manuscript received 7 April 2018; published 25 May 2018)

It is demonstrated that thermally induced atomic displacements from ideal lattice positions can produce considerable effect on magnetic exchange interactions and, consequently, on the Curie temperature of Fe. Thermal lattice distortion should, therefore, be accounted for in quantitatively accurate theoretical modeling of the magnetic phase transition. At the same time, this effect seems to be not very important for magnetic exchange interactions and the Curie temperature of Co and Ni.

DOI: 10.1103/PhysRevB.97.174426

I. INTRODUCTION

Accurate and reliable *ab initio* modeling of finite temperature properties of magnetic materials is a formidable problem in solid state physics and materials science. One of the major challenges is related to the absence of relevant thermal magnetic excitations in the routinely used version of density-functional theory (DFT) [1–3]. At the same time, proper many-body approaches to magnetic excitations [4–7] are highly computationally demanding, especially when nonlocal correlations are essential.

A more tractable approach is to map the initial quantum mechanical problem onto a semiclassical model, such as the Heisenberg model, whereby the necessary model parameters are obtained from a DFT calculation in the appropriate reference magnetic state. The magnetic thermodynamics, including the Curie temperature, are then described by a Monte Carlo or spin-dynamics simulation. Such an approach assumes that the magnetic degrees of freedom are well separated from other electronic excitations and lattice vibrations. Moreover, the timescale of magnetic excitations is typically much smaller than that of thermal lattice vibrations, which allows one to model magnetic thermodynamics on a fixed crystal structure.

The parameters of such Hamiltonians are obtained in first-principles calculations and may already include the contribution from the one-electron excitations. Besides, since the lattice vibrational excitations are generally slower than the magnetic ones, the effect of thermal lattice vibrations can be included in the first approximation by using the corresponding finite temperature lattice constant [8,9]. What is, however, missing in the latter case is the proper adiabatic coupling between magnetic excitations and lattice vibrations, as the magnetic problem is still considered on a fixed ideal lattice of the system.

Clearly, this coupling can be important at high temperatures, close to the melting transition. In particular, it has been demonstrated that thermal atomic displacements at temperatures close to the melting transition affect the electronic structure and bonding in Mo, substantially changing the relative stability of different crystal structures [10]. Recently, the effect of the thermal atomic motion on the one-electron excitations has been thoroughly studied by Zhang *et al.* [11]. Again, in some cases the effect is quite large, although it is relatively small at the temperature equal to the half of the melting temperature. Also, the so-called disordered-local-moment molecular dynamics (DLM-MD) simulations by Alling *et al.* [12] have revealed a large impact of thermal lattice displacements upon the electronic structure and local magnetic moments in Fe under a certain constraint on the spin configuration. Specifically, the electronic structure, particularly electronic and magnetic energies, of the bcc and fcc phases turned out to be almost indistinguishable at temperatures close to the melting point.

In this paper, we consider the effect of thermal lattice displacements on the magnetic phase transition in bcc Fe, fcc Co, and fcc Ni, assuming adiabatic coupling of magnetic excitations to the thermal atomic motion. Among these three materials, fcc Co has the largest ratio of Curie ($T_c = 1400$ K) and melting ($T_m = 1770$ K) temperatures, $t_c = 1400/1770 \approx 0.79$, followed by bcc Fe with $t_c = 1044/1811 \approx 0.58$ and by fcc Ni with $t_c = 630/1730 \approx 0.36$. One would expect Co to experience the largest impact of lattice vibrations on magnetic properties. We show that in contrast to this naive expectation, the strongest effect is observed in bcc Fe, where the adiabatic lattice-magnetic coupling reduces the theoretical Curie temperature by more than 30%. More so, a similar effect, although to a much smaller extent, is observed even in fcc Ni with its relatively low Curie temperature.

Our results are somewhat contradictory to the previous work of Yin *et al.* [13], who found that thermal lattice vibrations have very little effect on the Curie temperature, although they produce a noticeable shift of the heat capacity relative to the case when lattice vibrations and magnetic excitations are decoupled. The magnetic exchange interactions in those calculations have been obtained in supercell first-principles calculations with atomic positions from classical molecular dynamics (MD) simulations and for a magnetic configuration with randomly assigned spin directions. A possible origin of the difference with our results will be discussed below.

II. METHODOLOGY

A. Magnetic model

All metals considered here are band ferromagnets exhibiting various degrees of localization and itineracy: While bcc Fe is mainly on a localized side, fcc Co, and, especially, Ni are itinerant ferromagnets [14]. This determines our choice of the models of the magnetic state close to the magnetic phase transition as described below. However, since the magnetic phase transition in these metals is largely related to the reorientation of the local magnetic moments, it is determined in the statistical simulations, using the simplest form of the Heisenberg Hamiltonian:

$$H = -\sum_{i,j} J_{ij}\mathbf{e}_i\mathbf{e}_j, \tag{1}$$

where $\mathbf{e}_i$ is the direction of the magnetic moment at site i; J_{ij} are the magnetic exchange interaction parameters for a pair of atoms at sites i and j. The interaction parameters are obtained in the relevant state [8,9], i.e., taking into consideration the external and internal parameters of metals, including the lattice constant and the magnetic state at a finite temperature near the magnetic transition.

Specifically, the magnetic exchange interactions were determined at the Curie temperature experimental lattice constants: 2.904 Å in bcc Fe, 3.595 Å in fcc Co, and 3.543 Åin fcc Ni [15]. The same lattice constants were also used in the MD simulations, providing atomic configurations of these metals at the Curie temperature. The magnetic exchange interactions were calculated in the paramagnetic state (PM) [16]. However, we used different models of the paramagnetic state for different metals.

In the case of Fe, we assumed the localized behavior of magnetic moments, neglecting longitudinal spin fluctuations (LSF). This is a qualitatively reasonable model for bcc Fe since its magnetic moments in the ferromagnetic (FM) and PM states are rather similar: ∼2.2 and ∼2.0 μ_B, respectively. In calculations of the magnetic interaction parameters, we used the disordered local moments (DLM) approach [17] as described below.

On the contrary, the magnetic moment of fcc Co and Ni are very sensitive to the magnetic state [18]. In particular, the magnetic moment of Ni vanishes in the straightforward DLM modeling [19], while in Co it drops from ∼1.7μ_B in the FM state to ∼1.0 μ_B in the DLM state (for the high-temperature lattice constant). Therefore, in these metals, LSF play an important role at high temperature in the paramagnetic state and they should be accounted for in an appropriate way.

Here, we include them by minimizing the free energy of the DLM-LSF state by assuming that its entropy is [20]

$$S^{\mathrm{LSF}} = 3\ln(m), \tag{2}$$

where m is the average magnitude of the local magnetic moment, which is valid in the high-temperature limit when the LSF energy has a quadratic form. We also include the one-electron excitations at the corresponding Curie temperatures through the Fermi-Dirac distribution function.

B. Exchange-interaction-parameter calculations

The magnetic exchange interaction parameters were calculated within the Green's-function exact muffin-tin orbital (EMTO) method [21] using the magnetic force theorem [22]. In particular, the Lyngby version [23] of the EMTO code was used, which includes an efficient treatment of the magnetic disorder and LSF. The DLM and DLM-LSF calculations were done in the coherent potential approximation (CPA) [24]. The basis functions in the calculations were expanded up to $l_{\max} = 2$ but, for some of the cases presented below, results were obtained using $l_{\max} = 3$ to test the convergence. To provide a better convergence with partial waves, the blowing-up technique up to $l = 4$ was used in all the EMTO calculations [21]. The integration over the irreducible part of the Brillouin zone was performed using the Monkhorst-Pack grid [25], corresponding to the 36×36×36 for the primitive-unit cells. The local density approximation [26], was used in the self-consistent calculations.

C. Finite temperature atomic structures

Atomic configurations at the Curie temperatures were obtained in *ab initio* MD simulations by the projector augmented wave (PAW) method [27,28] as implemented in the Vienna *ab initio* simulation package (VASP) code [29–31]. For Co and Ni, we used a 32-atom 2×2×2 supercell built upon the cubic 4-atom fcc unit cell, while for Fe we used 54-atom (3×3×3) and 16-atom (2×2×2) supercells based on the bcc cubic 2-atom unit cell.

The NVT-ensemble MD simulations were carried out in a canonical ensemble using the algorithm of Nose [32]. The representative atomic configurations were chosen from the MD runs separated by at least 1 000 MD steps at temperatures close to the corresponding Curie temperatures. The time step was set to 2 ps in all the MD simulations. The 4×4×4 Monkhorst-Pack grid [25] was used in the Brillouin zone integration for the fcc 32-atom and bcc 54-atom supercells, while the 8×8×8 grid was used for the 16-atom bcc supercell. Generalized gradient approximation in the Perdew-Burke-Ernzerhof (PBE) parametrization [33] was used in the PAW calculations.

As mentioned above, the lattice constants were chosen to be equal to the experimental ones at the point of the magnetic phase transition. The MD calculations were done in the FM state. It seems that this is the only way to have reasonable magnitudes of the local magnetic moments and thus equilibrium volumes close to the experimental ones. The latter is supported by the fact that the total average pressure in calculations was found to be −13.9, −23.7, and 1.8 kB for Co, Fe, and Ni, respectively. The use of the FM state in MD simulations is important not only in the cases of fcc Ni and Co, but also in the case of bcc Fe, as will be discussed below.

To check if such MD simulations provide a reasonable account for the thermal lattice displacements at the corresponding Curie temperatures, we have also calculated the mean square atomic displacements in all three systems. They are 0.042, 0.022, and 0.066 Å^2 for Fe, Ni, and Co, respectively. The results for Fe and Ni are in reasonable agreement with model estimates from the experimental Debye-Waller factors [34]: 0.05 and 0.03 Å^2, respectively. We have not been able to

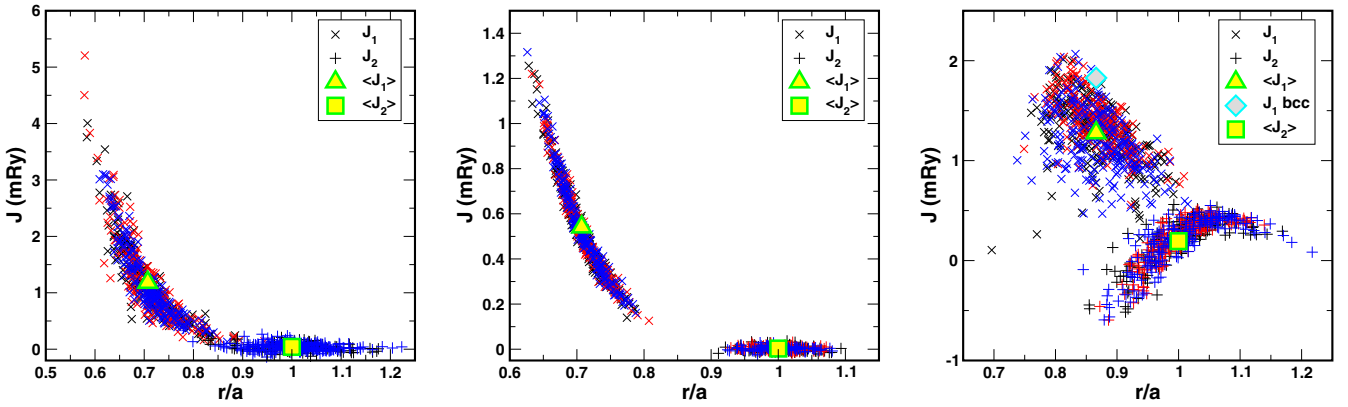

FIG. 1. Magnetic exchange interaction parameters of Co (left), Ni (center), and Fe (right) at the first two coordination shells for three different MD snapshots marked by blue, red, and black colors (32-atom supercells in the case of Co and Ni and 54-atom supercell in the case of Fe, as described above). The distances are given in units of a lattice constant, a. The paramagnetic state in Co and Ni is modeled with LSF-DLM, while in Fe using conventional DLM approach.

find data for fcc Co. However, the result for Co seems to be reasonable, taking into consideration the proximity of its Curie temperature to the melting point.

III. RESULTS

A. Magnetic exchange interactions

In Fig. 1, we show the magnetic exchange interaction parameters obtained from the EMTO calculations for the MD snapshots at the first two coordination shells for Co, Ni, and Fe. One can notice that the thermal lattice displacements are quite large in all simulations, which leads to the substantial deviation of the magnetic exchange interactions for certain pairs of atoms, even in the case of Ni at a relatively low temperature 630 K. One can also see that for Co and Ni, the interactions are mostly affected by the interatomic distance, while in the case of Fe the behavior of the magnetic exchange interactions looks more complicated with a large dispersion of their values close to the nearest-neighbor distance of the ideal bcc structure, $r_{1-\mathrm{bcc}} = a/\sqrt{3} \approx 0.87a$.

In Fig. 2, we compare the average magnetic exchange interactions for the first few coordination shells in different MD samples and the corresponding ideal structures (for specific values, see Tables I and II in the Appendix). Taking into consideration the restricted size of the MD samples and the number of MD samples, we can talk only about qualitative effects. Nevertheless, the effect of thermal lattice displacements is clearly noticeable in the cases of Co and Fe. In particular, there is a pronounced change of the magnetic exchange interactions of Co at the first, third, and fourth coordination shells, which provide the strongest contribution to T_c.

The most dramatic effect is observed in the case of Fe for the nearest-neighbor magnetic exchange interactions, J_1, whose values in the MD samples drop by about 30% on average from the value for the ideal bcc structure. What is quite unexpected, however, is that the nearest-neighbor interaction in the ideal bcc structure appears to be almost on top of all the interactions in the MD samples at $r_{1-\mathrm{bcc}}$. Clearly, the magnetic exchange interactions in Fe are very sensitive not only to the corresponding interatomic distances but also to the deviation of the local structure from the ideal bcc one.

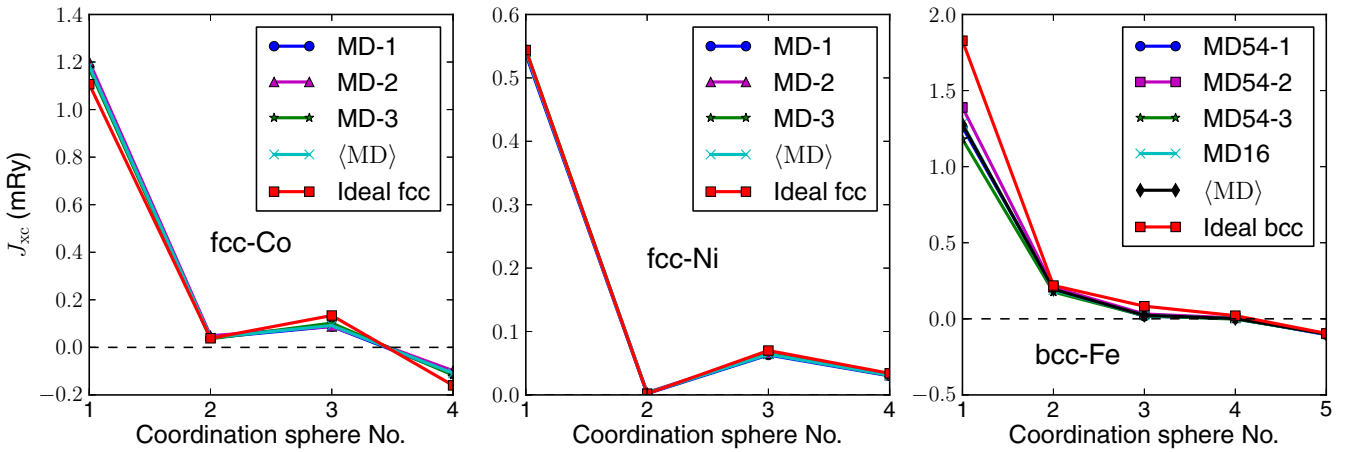

FIG. 2. Magnetic exchange parameters at the first few coordination shells for Co (left), Ni (center), and Fe (right) obtained in various MD snapshots. The parameters for the snapshots are obtained as averages over atomic pairs corresponding to a given coordination shell. ⟨MD⟩ denotes an average over snapshots 1, 2, 3.

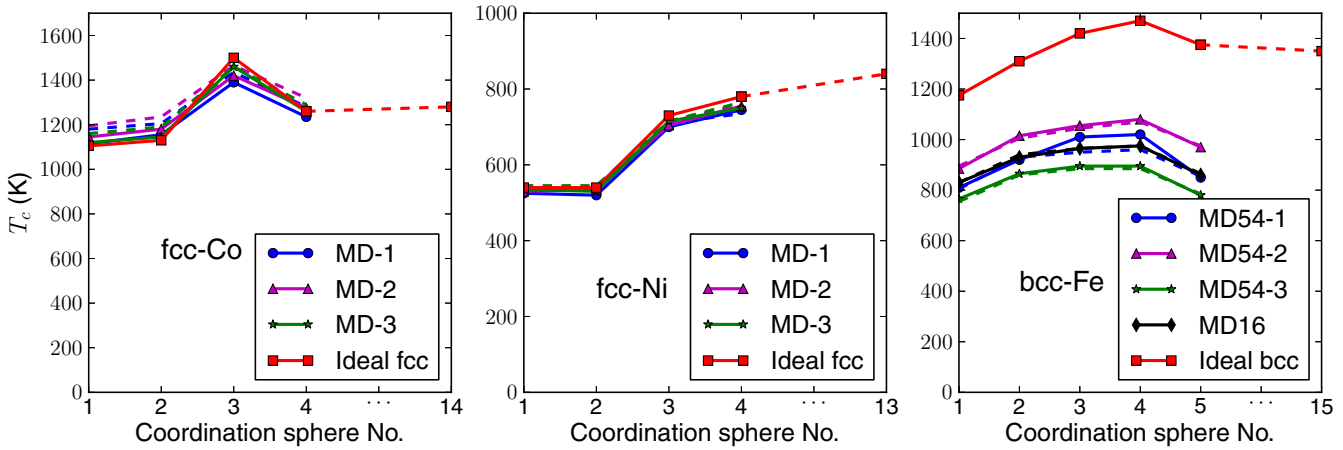

FIG. 3. Curie temperatures for Co (left), Ni (center), and Fe (right) as obtained from MC simulations with parameters obtained in various MD snapshots (see text). For each snapshot, a solid line corresponds to the values obtained using actual magnetic exchange parameters (setup 1) and a dashed line corresponds to averaged magnetic exchange parameters (setup 2). The purpose of a dashed segment in the plot of T_c for an ideal structure (setup 3) is to show convergence with respect to coordination shells.

Our results for magnetic exchange interactions in Fe MD samples presented in Fig. 1 are actually qualitatively very similar to the results of Ref. [13] obtained in the LSMS calculations. However, there is a quantitative difference because of different methodologies employed: while a random configuration of magnetic spins have been used in the calculations of magnetic exchange interactions in Ref. [13], it is not equivalent to the DLM-CPA model used here, which provides a homogeneously random presentation of the paramagnetic state as discussed below. As to the qualitative similarity, our calculations of the magnetic exchange interactions in the FM state produce results similar to the ones in the DLM state and to those presented in Ref. [13] as well as in Ref. [35], where an amorphouslike structure was considered. This suggests that this behavior of magnetic interactions in Fe is generic.

B. Curie temperature

The Curie temperature calculations were performed by the Monte Carlo (MC) method. $8\times8\times8$ supercells of the 32-atom unit cells representing snapshots of the MD simulations were used in MC simulations in the case of Co and Ni, while for the ideal fcc structure for these metals a $16\times16\times16$ supercell was used built upon the 4-atom fcc cubic unit cell. Similarly, in the case of Fe, $8\times8\times8$ supercells of the 54-atom MD snapshots and a $20\times20\times20$ supercell of the 2-atom bcc cubic unit cell were used in the MC simulations.

The number of MC steps for the thermalization of spin configurations was 20 000 and measurements were performed during the next 25 000 MC steps at each temperature. The temperature step was 5 K in all MC simulations. The Curie temperature was identified by the peak of the heat capacity, which is sufficiently accurate for a semiquantitative consideration. A more precise calculation would require averaging over MD samples, which has not been done because this goes beyond the purpose of this paper.

For every metal, we obtain the Curie temperature within three different setups:

(1) Actual MD snapshots with the magnetic exchange parameters as obtained in EMTO calculations for every pair of atoms (see Fig. 1);

(2) Supercells based on ideal crystal lattices (bcc or fcc) with the interactions obtained from MD snapshots by averaging over atomic pairs (shown in Fig. 2 and in Tables I and II in the Appendix);

(3) Supercells based on ideal crystal lattices with the interactions obtained for the corresponding ideal structure.

The results for the Curie temperatures are presented in Fig. 3 (for specific values see Tables III and IV in the Appendix). First of all, one can see that the Curie temperature obtained for actual MD snapshots can deviate noticeably from that for a corresponding ideal structure. This result is independent of whether we use inhomogeneous magnetic exchange interactions (setup 1) or the ones averaged over atomic pairs (setup 2). The difference between these two setups is, in fact, smaller than the sample-to-sample variation, especially pronounced in Co and Fe.

The strongest deviation from the ideal-structure values is observed in Fe, in which T_c drops by about 400 K due to thermal lattice displacements. This effect could have already been inferred from the significant reduction of J_1 (rightmost panel in Fig. 2). Another important observation is an appreciable sample-to-sample variation ($\sim$200 K) of the Curie temperature, which might be due to the neglect of LSF in the current modeling of the paramagnetic state of Fe. Nevertheless, it is clear that the magneto-lattice coupling is quite strong in this case and an accurate *ab initio* modeling of the magnetic transition in Fe should account for the thermal lattice displacements.

In contrast to the case of Fe, the results on T_c in Co might appear surprising at first sight. As seen in the left panel of Fig. 2, the magnetic exchange interaction at the first coordination shell, J_1, experiences an enhancement by almost 10l% due to thermal atomic displacements. Given the high value of T_c in the ideal structure, this could have resulted in a systematic increase of the Curie temperature in the MD samples. And indeed, this can be seen in the MC with only J_1 taken into

account (left panel of Fig. 3). However, as more coordination shells are included, the increase of T_c practically vanishes (see also values in Table III in the Appendix). This can also be traced back to the exchange parameters, which reveal that the reduced absolute values at the third and fourth coordination shells have a compensating effect on the final value of the Curie temperature. As a result, one may conclude that, despite their large amplitude (up to 25% of the NN distance), thermal atomic displacements play a relatively little role in the magnetic transition in Co.

In this respect, a small but systematic reduction of T_c in Ni seems unexpected. Unlike Co, the ratio of the Curie to the melting temperature is quite small here (∼36%) and the amplitude of the thermal atomic displacements is no more than 16%. Also, the values of J_1 for MD snapshots are practically indistinguishable from the ones for the ideal lattice. Nevertheless, a small systematic reduction of magnetic interactions at higher coordination shells is sufficient to have a noticeable impact on T_c.

IV. DISCUSSION

The values of exchange interactions J_{ij} parametrizing Hamiltonian Eq. (1) already include the magnitudes of the local magnetic moments. It is thus tempting to ascribe the behavior of the exchange interactions described above to the variations of local magnetic moments induced by the thermal lattice distortions. Below we consider the local magnetic moments in MD samples of Fe and show that, as a matter of fact, such variations are rather small and cannot be responsible for the strong effect of lattice vibrations on the exchange interactions.

The subsequent subsection is devoted to a more detailed analysis of the trends observed in the behavior of J_{ij}. In particular, we discuss the distance dependence of the magnetic interactions.

A. Local magnetic moments

As has been mentioned above, the MD simulations were done in the FM state. The reason is that all the considered metals are band ferromagnets, whose magnetic moments are very sensitive to the atomic structure and especially to the magnetic state within the usual DFT calculations without LSF. At the same time, in the paramagnetic state with LSF, the latter are mostly responsible for the magnitudes of the local magnetic moments, which become much more sensitive to the temperature than to the local atomic and magnetic structure structure. Since the LSF cannot be included in the DFT-MD calculations using VASP, the best way to provide stable magnetic moments is to use the FM state as a magnetic configuration.

Subsequent EMTO-CPA calculations of the DLM-LSF magnetic moments in the MD samples show that this is indeed the case. For instance, the average DLM-LSF magnetic moments in Co and Ni, which are 1.58 μ_B and 0.68 μ_B, are very close to the average local magnetic moments in the FM state, which are 1.69 and 0.62 μ_B, respectively. Besides, the dispersion of local magnetic moments in the DLM-LSF state is quite small: the magnetic moments of Co in all three MD samples are between 1.50 and 1.65 μ_B (the average magnitude is 1.58 μ_B) and in Ni the deviation from the average magnetic moment does not exceed 0.02 μ_B.

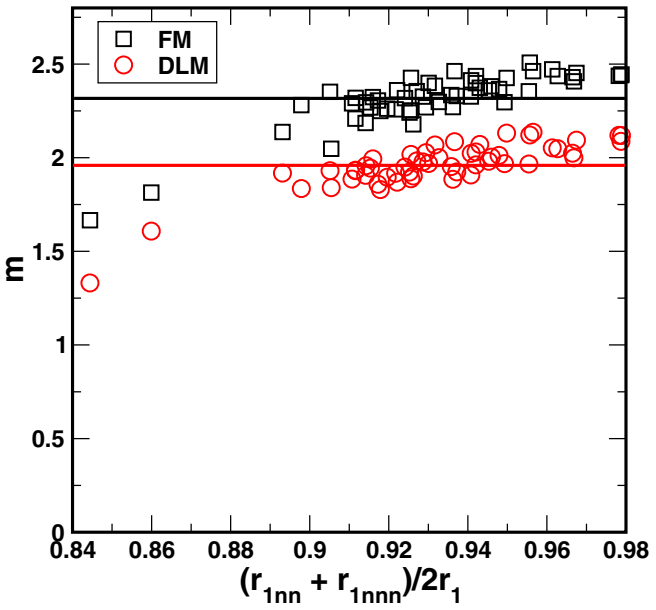

FIG. 4. Local magnetic moments in one of the MD snapshots obtained in the EMTO FM and DLM calculations The thick lines indicate the average magnitude of magnetic moment in both cases. Here, r_{nn} and r_{nnn} are the distances to the nearest neighbor and next-nearest neighbor atoms for a particular atom in the sample, and r_1 is the radius of the first coordination shell in the ideal bcc structure.

Although the situation is a bit different in Fe, where LSF are neglected in the DLM EMTO-CPA calculations, the effect of the local atomic displacements on the magnitude of local magnetic moments is relatively small too. In Fig. 4, we show local magnetic moments obtained from EMTO calculations in the FM and DLM states for one of the MD samples of Fe having the largest dispersion of the magnitudes of the magnetic moments. They are shown as functions of the average of the shortest and next-shortest distance between a particular atom and its two neighbors, which corresponds to the first coordination shell in the ideal bcc structure. The distances are normalized by the nearest-neighbor distance in the ideal bcc structure.

One can see that the magnetic moments of only two atoms deviate relatively strongly from the corresponding average magnitudes. In fact, these two atoms form a nearest-neighbor pair with the shortest interatomic distance (r_{nn}/r_{1-bcc}=0.804) out of all three MD samples. In all the other samples, the lowest magnitudes of the local magnetic moments in the DLM state are 1.84, 1.78, and 1.84 μ_B. Thus, even in the case of DLM calculations without additional enhancement by the LSF, the magnitude of the magnetic moments exhibits a relatively small dispersion.

These results for the local magnetic moments of Fe in the DLM state for a MD sample are in stark contrast to the results of the so-called DLM-MD simulations presented in Ref. [12], where the local magnetic moments deviate strongly from their average values and vanish almost completely on some of the atoms. The reason for such a dramatic difference in the results is related to the way a DLM-like constraint is imposed in

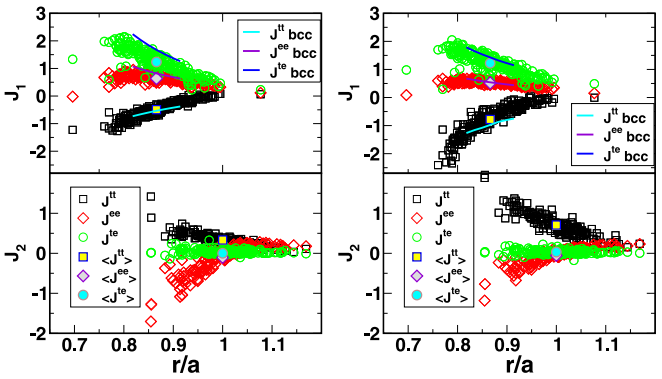

FIG. 5. Orbital decomposition of the magnetic exchange interactions in one of the Fe MD snapshots at the first two coordination shells in the DLM (left) and FM (right) state. t stands for t_{2g}, e for e_g. Black boxes denote t_{2g}-t_{2g} sector, red diamonds—e_g-e_g sector, and green circles—mixed t_{2g}-e_g sector (see legend).

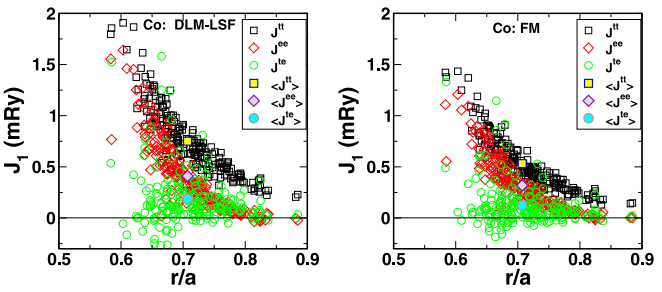

FIG. 6. Orbital decomposition of the magnetic exchange interactions in one of Co MD snapshots at the first coordination shell in the DLM-LSF (left) and FM (right) state.

the DLM-MD approach. Specifically, while a distribution of spin-up and spin-down atoms in a MD sample mimics complete disorder on average, the spin configuration is *static* at any given point of time, which results in very unfavorable local magnetic environment (e.g., with an ordered antiferromagnetic pattern on nearest neighbors) for some of the atoms. The magnetic moments of such atoms will then be appreciably reduced or completely suppressed in a strongly distorted bcc structure because of the relatively "soft" and itinerant nature of magnetism in Fe. Let us also note that we do not expect that increasing the supercell size in the DLM-MD approach is going to improve the behavior because the main problem of the method is the violation of timescale separation for vibrational and magnetic degrees of freedom.

On the contrary, in a genuine DLM-CPA calculation, each atom "sees" a time-averaged spin configuration. Effective time averaging (replaced by the configurational averaging within CPA) is what distinguishes the DLM-CPA approach from supercell calculations with static random spin distributions.

B. The origin of trends in magnetic exchange interactions

There is a very clear qualitative difference in behavior of exchange interactions between Fe and Co/Ni. Ni can be considered as the simplest case here, in which the exchange integrals depend only on distances between pairs of atoms. This reflects the itinerant character of magnetism with a weak momentum dependence of the spin susceptibility.

Iron, on the other hand, is known to have a much stronger momentum dependence of magnetic correlations [36], which leads to a much more pronounced sensitivity of the exchange interactions to deviations of bond directions from their ideal positions in the bcc structure. Such a behavior implies a strong orbital dependence of the magnetic response. And indeed, this is what we observe when we decompose $J_{\rm xc}$ into orbital contributions, as shown in Fig. 5. In agreement with previous studies [37–39], the t_{2g} and e_g terms contribute with different signs at the first two coordination shells, while the positive value of J_1 is largely determined by the strong t_{2g}-e_g term, $J^{te} \equiv J^{t_{2g}-e_g}$. Moreover, it is the latter contribution that exhibits the strongest dependence on the deviation of thermally disordered local structure from the ideal one. The interaction parameter at the second coordination shell has a negligible t_{2g}-e_g contribution, which is clear because in the ideal bcc structure this term is forbidden by symmetry. The value of J_2 is thus mainly determined by the t_{2g} term. This is consistent with the observation made in Ref. [39], that the magnetic interaction associated with t_{2g} states are determined by the Fermi surface and has long range. In contrast, the e_g term has a localized (tight-binding) character and it is short range.

The behavior of exchange interactions in Co is similar to that of Ni, with a slight tendency toward the localized behavior inherent to Co. The orbital decomposition shown in Fig. 6 reveals that t_{2g} and e_g contributions are almost the same at the first coordination shell, which one would expect from an itinerant ferromagnet. The interorbital term J^{te} shows a strong direction dependence, but unlike Fe, its contribution to the exchange integral is rather small (less than 20%).

Despite disorder in atomic positions, the exchange interactions exhibit a clear dependence on the distance between pair of atoms. At the same time, one should be careful in defining $J_{\rm xc}$ as a simple function of the distance, as it is often done in model studies. For instance, by comparing the left and right panels of Fig. 5, one can see that the distance dependence is obviously different for different magnetic states (FM or DLM). Moreover, even for a given magnetic state the exchange interactions depend on other aspects of the electronic state, such as, e.g., average electron density.

To demonstrate this, we calculate $J_{\rm xc}$ for the ideal bcc structure as a function of volume, constraining the magnetic moment to the one at the equilibrium volume. The resulting interactions are shown as solid lines overlaying the scatter plots in Fig. 5. Apart from the already pointed-out difference between ideal-structure and MD-averaged values, it is clear that the distance-dependence of the interactions in MD snapshots is noticeably different from the one observed for J_{xc} obtained as functions of volume. This discrepancy is especially pronounced in the DLM state (left panel of Fig. 5), where $J_1^{e_g-e_g}$ as a function of volume shows an upward trend at small distances but the corresponding interaction in a MD-snapshot has a clear maximum around $r = 0.8a$. Given the weak variation in the magnetic moments (Fig. 4) this tells us that the magnetic exchange parameters are not only dependent on the magnetic state, which has long been known, but they are also affected by other quantities characterizing the electronic state (e.g., electron density).

TABLE I. Average magnetic exchange interactions (mRy) in Co and Ni (DLM-LSF state) for the MD simulation samples and in the ideal fcc structure at the experimental Curie temperatures and lattice constants. The last column shows the effect of the basis on the magnetic exchange interactions in the EMTO calculations.

C.s.	MD-1	MD-2	MD-3	⟨**MD**⟩	**fcc**	fcc ($l_{max}=3$)
			Co			
1	1.177	1.202	1.172	**1.183**	**1.107**	1.097
2	0.040	0.049	0.036	**0.041**	**0.038**	0.033
3	0.088	0.088	0.102	**0.092**	**0.134**	0.132
4	−0.111	−0.098	−0.117	**−0.109**	**−0.160**	−0.160
			Ni			
1	0.537	0.542	0.545	**0.541**	**0.544**	0.540
2	0.002	0.004	0.003	**0.003**	**0.002**	0.002
3	0.063	0.065	0.065	**0.064**	**0.070**	0.069
4	0.030	0.031	0.031	**0.031**	**0.034**	0.037

V. SUMMARY

We have developed a computational approach for simulating high-temperature magnetic-phase transition in itinerant magnets, which couples adiabatically thermal lattice distortions and magnetic excitations. This scheme consists of three computational steps: (1) *ab initio* MD simulations of the material at the given temperature, (2) first-principles calculations of magnetic exchange interactions in the given magnetic state within DFT, and (3) MC modeling of the magnetic transition.

It has been applied here to calculations of the Curie temperature in bcc Fe, fcc Co, and fcc Ni. The atomic configurations have been obtained from the AIMD simulations in the FM state at a temperature close to the Curie temperature. The MD samples have been used for the calculations of the magnetic exchange interactions in the paramagnetic state modeled by DLM for Fe and DLM-LSF in the case of Co and Ni. Although the thermal atomic displacements lead to a large dispersion of the magnetic exchange interactions in these metals, the strongest effect on the average exchange interactions is in Fe, which results consequently in the large drop of the Curie temperature. This implies that an accurate modeling of the thermodynamic properties of bcc Fe close to above the Curie temperature should take thermal lattice displacements into account.

We also show that, at least in Fe, the magnetic exchange parameters are not simple functions of the distance but they generally dependent on other parameters of the electronic structure. Although this information is not new *per se*, we demonstrate here clearly that the distance-dependence of J_{xc} obtained from a MD snapshot for a fixed volume is different from that obtained from a calculation for the ideal structure as a function of volume.

TABLE III. The Curie temperature (Kelvins) of Co and Ni as a function of the coordination shells included in the MC simulations. The value in parentheses is the Curie temperature obtained for the ideal fcc structure using the average magnetic exchange interaction parameters. The last two columns present the results for the ideal underlying structure using interactions from Table I.

C.s.	MD-1	MD-2	MD-3	fcc	fcc ($l_{max}=3$)
			Co		
1	1115 (1180)	1145 (1195)	1120 (1160)	1105	1095
2	1155 (1205)	1180 (1235)	1145 (1190)	1130	1105
3	1390 (1435)	1420 (1465)	1460 (1460)	1500	1470
4	**1235** (1280)	**1275** (1320)	**1260** (1290)	**1260**	1235
14	–	–	–	**1280**	1265
			Ni		
1	525 (535)	530 (540)	535 (545)	540	540
2	520 (535)	535 (540)	530 (545)	540	540
3	700 (710)	705 (715)	715 (715)	730	730
4	**745** (735)	**755** (760)	**750** (765)	**780**	780
13	–	–	–	**840**	840

ACKNOWLEDGMENTS

The author acknowledges the support of the Swedish Research Council (VR Project No. 2015-05538), a European Research Council grant, the VINNEX center Hero-m, financed by the Swedish Governmental Agency for Innovation Systems (VINNOVA), Swedish industry, and the Royal Institute of Technology (KTH). Calculations were done using NSC (Linköping) and PDC (Stockholm) resources provided by the Swedish National Infrastructure for Computing (SNIC). The support from the Austrian federal government (in particular from Bundesministerium für Verkehr, Innovation und Technologie and Bundesministerium für Wirtschaft, Familie und Jugend) represented by Österreichische Forschungsförderungsgesellschaft mbH and the Styrian and the Tyrolean provincial government, represented by Steirische Wirtschaftsförderungsgesellschaft mbH and Standortagentur Tirol, within the framework of the COMET Funding Programme is also gratefully acknowledged.

APPENDIX

In the Appendix, we provide tables containing the results of calculations. Tables I and II present the magnetic exchange

TABLE II. Average magnetic exchange interactions (mRy) in Fe (DLM state) for the MD simulation samples and in the ideal bcc structure at the experimental Curie temperature and lattice constant.

C.s.	MD54-1	MD54-2	MD54-3	MD-16	⟨**MD**⟩	**bcc**	bcc ($l_{max}=3$)
1	1.260	1.389	1.180	1.284	**1.277**	**1.828**	1.818
2	0.202	0.207	0.176	0.189	**0.194**	**0.219**	0.189
3	0.017	0.032	0.020	0.022	**0.023**	**0.083**	0.082
4	0.003	0.006	−0.002	0.002	**0.002**	**0.021**	0.021
5	−0.104	−0.099	−0.098	−0.100	**−0.100**	**−0.096**	−0.097

TABLE IV. The Curie temperature of Fe as a function of coordination shells included in the MC simulations similar to Table III. The last two columns present the results for the ideal underlying structure using interactions from Table II.

C.s.	MD54-1	MD54-2	MD54-3	MD16	bcc	bcc ($l_{\max} = 3$)
1	810 (805)	885 (895)	765 (755)	830 (830)	1175	1165
2	920 (930)	1015 (1005)	865 (860)	930 (940)	1310	1285
3	1010 (950)	1055 (1045)	895 (885)	965 (965)	1420	1380
4	1020 (960)	1080 (1070)	895 (885)	975 (975)	1470	1455
5	**850** (855)	**970** (975)	**780** (785)	**860** (865)	**1375**	1360
15	–	–	–	–	**1350**	1300

parameters at the first several coordination shells for Co, Ni, and Fe. The supercell-averaged interactions are shown for various MD snapshots (for details, see Sec. II C). Also, the values for a higher l-cutoff of the EMTO basis are given to demonstrate convergence with respect to $l_{\max}$. It is clear that the error related to the l-cutoff is much smaller than the difference between MD-snapshot and ideal-lattice values.

By comparing the typical values of the exchange parameters averaged over MD snapshots with those of an ideal structure, one can see that there is a strong reduction of the MD-averaged interactions at the first coordination shell in the case of Fe. This is in contrast to the case of Co, where the effect is very small. In Ni, the difference between the MD-averaged and ideal exchange parameters is even weaker but, as seen below, it results in a small but systematic reduction of the simulated Curie temperature.

Tables III and IV show the Curie temperatures extracted from MC simulations with magnetic exchange interactions obtained for MD snapshots or for ideal structures. For MD snapshots, only exchange parameters for the first several (4–5) coordination shells are taken into account. To make sure that this is sufficient for convergence, we use T_c of an ideal structure calculated with a large number of coordinations shells as a reference. Also, values of T_c obtained with exchange parameters averaged over an MD snapshot are shown in the parentheses to demonstrate that the inhomogeneity of actual snapshot interactions plays only a little role (mostly noticeable in the case of Co).

[1] W. Hohenberg and P. Kohn, Phys. Rev. **136**, B864 (1964).
[2] W. Kohn and L. J. Sham, Phys. Rev. **140**, A1133 (1965).
[3] N. D. Mermin, Phys. Rev. **137**, A1441 (1965).
[4] A. I. Lichtenstein, M. I. Katsnelson, and G. Kotliar, Phys. Rev. Lett. **87**, 067205 (2001).
[5] V. I. Anisimov, A. S. Belozerov, A. I. Poteryaev, and I. Leonov, Phys. Rev. B **86**, 035152 (2012).
[6] A. S. Belozerov, I. Leonov, and V. I. Anisimov, Phys. Rev. B **87**, 125138 (2013).
[7] A. S. Belozerov and V. I. Anisimov, J. Phys.: Condens. Matter **26**, 375601 (2014).
[8] A. V. Ruban, S. Shallcross, S. I. Simak, and H. L. Skriver, Phys. Rev. B **70**, 125115 (2004).
[9] A. V. Ruban, Phys. Rev. B **95**, 174432 (2017).
[10] C. Asker, A. B. Belonoshko, A. S. Mikhaylushkin, and I. A. Abrikosov, Phys. Rev. B **77**, 220102 (2008).
[11] X. Zhang, B. Grabowski, F. Körmann, C. Freysoldt, and J. Neugebauer, Phys. Rev. B **95**, 165126 (2017).
[12] B. Alling, F. Körmann, B. Grabowski, A. Glensk, I. A. Abrikosov, and J. Neugebauer, Phys. Rev. B **93**, 224411 (2016).
[13] J. Yin, M. Eisenbach, D. M. Nicholson, and A. Rusanu, Phys. Rev. B **86**, 214423 (2012).
[14] T. Moriya, *Spin Fluctuations in Itinerant Electron Magnetism* (Springer, Berlin, 1985).
[15] M. B. Stearns, in *Landolt-Börnstein—Group III Condensed Matter*, edited by H. Wijn (Springer-Verlag, Berlin, Heidelberg, 1986), Vol. 19A, p. 24.
[16] It is worth noting the paramagnetic state close to the Curie temperature is characterized by a magnetic short range order with a large correlation length and the value of the spin-spin correlation function of about 0.3 at the first coordination shell. That being said, calculations for a ferromagnetic state with magnetization of 0.2–0.3, which mimics to some extent this magnetic short range order, show that the magnetic exchange interactions remain very close to the ones obtained in the completely disordered paramagnetic state.
[17] B. L. Gyorffy, A. J. Pindor, J. Staunton, G. M. Stocks, and H. Winter, J. Phys. F **15**, 1337 (1985).
[18] S. Shallcross, A. E. Kissavos, V. Meded, and A. V. Ruban, Phys. Rev. B **72**, 104437 (2005).
[19] A. V. Ruban, S. Khmelevskyi, P. Mohn, and B. Johansson, Phys. Rev. B **75**, 054402 (2007).
[20] A. V. Ruban, A. B. Belonoshko, and N. V. Skorodumova, Phys. Rev. B **87**, 014405 (2013).
[21] L. Vitos, Phys. Rev. B **64**, 014107 (2001); L. Vitos, I. A. Abrikosov, and B. Johansson, Phys. Rev. Lett. **87**, 156401 (2001).
[22] A. Liechtenstein, M. Katsnelson, V. Antropov, and V. Gubanov, J. Magn. Magn. Mater. **67**, 65 (1987).
[23] A. V. Ruban and M. Dehghani, Phys. Rev. B **94**, 104111 (2016).
[24] B. L. Györffy and G. M. Stocks, in *Electrons in Disordered Metals and at Metallic Surfaces*, edited by P. Phariseau, B. L. Györffy, and L. Scheire (Springer US, Boston, MA, 1979), pp. 89–192.
[25] H. J. Monkhorst and J. D. Pack, Phys. Rev. B **13**, 5188 (1976).
[26] J. P. Perdew and Y. Wang, Phys. Rev. B **45**, 13244 (1992).
[27] P. E. Blöchl, Phys. Rev. B **50**, 17953 (1994).
[28] G. Kresse and D. Joubert, Phys. Rev. B **59**, 1758 (1999).
[29] G. Kresse and J. Hafner, Phys. Rev. B **47**, 558 (1993).
[30] G. Kresse and J. Hafner, Phys. Rev. B **49**, 14251 (1994).

[31] G. Kresse and J. Furthmüller, Phys. Rev. B **54**, 11169 (1996).
[32] S. Nosé, J. Chem. Phys. **81**, 511 (1984); Prog. Theor. Phys. Suppl. **103**, 1 (1991).
[33] J. P. Perdew, K. Burke, and M. Ernzerhof, Phys. Rev. Lett. **77**, 3865 (1996).
[34] M. Kumar and M. P. Hemkar, Nuovo Cimento B **44**, 451 (1978).
[35] R. F. Sabiryanov, S. K. Bose, and O. N. Mryasov, Phys. Rev. B **51**, 8958 (1995).
[36] P. A. Igoshev, A. V. Efremov, and A. A. Katanin, Phys. Rev. B **91**, 195123 (2015).
[37] D. M. Korotin, V. V. Mazurenko, V. I. Anisimov, and S. V. Streltsov, Phys. Rev. B **91**, 224405 (2015).
[38] Y. O. Kvashnin, R. Cardias, A. Szilva, I. Di Marco, M. I. Katsnelson, A. I. Lichtenstein, L. Nordström, A. B. Klautau, and O. Eriksson, Phys. Rev. Lett. **116**, 217202 (2016).
[39] R. Cardias, A. Szilva, A. Bergman, I. D. Marco, M. I. Katsnelson, A. I. Lichtenstein, L. Nordström, A. B. Klautau, O. Eriksson, and Y. O. Kvashnin, Sci. Rep. **7**, 4058 (2017).